International Journal of Nanoelectronics and Materials
IJNeaM
ISSN 1985-5761 | E-ISSN 2232-1535

Comparative Analysis of Bovine Serum Albumin Detection Using Cuvettes, Biofunctionalized, and Non-Biofunctionalized Tapered Optical Fiber

Nur Nadia Bachok[a], Norhafizah Burham[b], Ahmad Razi Othman[c], Nurul Huda Abd Karim[d], Ahmad Ashrif A Bakar[a], Retna Apsari[e], and Norhana Arsad[a,*]

[a]*Photonics Technology Laboratory, Department of Electrical, Electronic and Systems Engineering, Faculty of Engineering and Built Environment, Universiti Kebangsaan Malaysia, 43600 UKM Bangi, Selangor, Malaysia*
[b]*Integrated Microelectronics System and Applications (IMSaA), School of Electrical Engineering, College of Engineering, Universiti Teknologi MARA, 40450 Shah Alam, Selangor, Malaysia*
[c]*Department of Chemical and Process Engineering, Faculty of Engineering and Built Environment, Universiti Kebangsaan Malaysia, 43600 UKM Bangi, Selangor, Malaysia*
[d]*Department of Chemical Science, Faculty of Science and Technology, Universiti Kebangsaan Malaysia, 43600 UKM Bangi, Selangor, Malaysia*
[e]*Department of Engineering, Faculty of Advanced Technology and Multidiscipline, Universitas Airlangga, Jl. Mulyorejo, Surabaya 60115, Indonesia*
**Corresponding author. Tel.: 03-8911-8363; e-mail: noa@ukm.edu.my*

Received 15 September 2023, Revised 1 October 2025, Accepted 27 October 2025

ABSTRACT

Advances in optical sensor technologies have been substantial in recent years, especially in the detection of biomolecules like Bovine Serum Albumin (BSA), driven by the need for more sensitive and precise diagnostic tools. The detection of BSA plays a critical role, particularly in the early diagnostic tools for chronic kidney disease. This work aims to investigate the performance of three different BSA detection methods: biofunctionalized and non-biofunctionalized tapered optical fiber sensors and conventional cuvettes. This study conducted an experimental investigation, utilizing a 3.5 ml cuvette and tapered optical fibers with design parameters including upper and lower taper lengths of 10 mm, a waist length of 10 mm, and a waist diameter of 10 μm. The sensors were fabricated using the Vytran GPX 3400 machine. Measurements of time response, intensity, and absorbance were carried out using a Deuterium-Tungsten DT-2-GS light source and an Ocean Optics Flame spectrometer. The biofunctionalization of the sensing area involved three sequential steps: hydroxylation with a 0.1M sodium hydroxide solution, salinization with a 2% (3-aminopropyl) triethoxysilane solution, and aldehyde activation using a 2% glutaraldehyde solution. The experiment used 120 ml of BSA solutions at concentrations of 31.25 mg/dL, 62.5 mg/dL, and 125 mg/dL. Each method exhibits a unique spectral response across the ultraviolet, visible, and near-infrared regions. Both intensity and absorbance assessments reveal a significant reduction in sensitivity when transitioning from the cuvette to the tapered optical fiber. Notably, the sensitivity decreases by 99.96% for intensity measurements and by 97.76% for absorbance. Nonetheless, after biofunctionalization, the tapered optical fiber's sensitivity increased, showing a 207.1% increase in absorbance and a 1494.72% increase in intensity measurements compared to the non-biofunctionalized tapered optical fiber.

Keywords: *Spectrometer, bovine serum albumin, intensity, absorbance, tapered optical fiber, biofunctionalized, biosensor*

1. INTRODUCTION

We have seen the great influence of optical technologies in many aspects of our life, such as security [1], [2], communication [3], [4], imaging [5], [6], and healthcare [7], [8]. The current development in optical sensor applications is very promising in regard to further innovations. Prominent examples of studies on this field are the development of temperature[9],, vibration[10], humidity [11],, and gas sensors [12]. All these sensors are enhancing accuracy, as well as productivity in their respective fields. Studies have always shown a huge possibility of the different bio-optical sensors, such as D-Fiber, U-Fiber, Fiber Bragg Gratings (FBG), Mach-Zehnder interferon meters as well as Surface Plasmon Resonance (SPR) sensors [13], [14]. The experimental studies conducted by multiple researchers have proven the fact that bio-optical sensors are highly sensitive and are also measurable. This is an exciting fact that opens new possibilities to explore how they can be put into use in the biosensors industry.

There is an increasing number of people affected by kidney related diseases [15]. Albuminuria has been used to measure kidney problems over several decades. Nevertheless, in the paper by Teeuw et.al (2021) and Mejia et al. (2022), the existing detection resources based on the urine dipstick approach are demonstrated to be ineffective [16], [17].. Moreover, Thakur (2021) emphasizes that urine dipstick based on paper reveals the presence of albumin based on color changes, which provide semi quantitative and insensitivity especially when the concentration is lower than 300 mg/dL [18]. Collectively, these studies can favor the idea on the identification of new options to fix and measure albumin. The growing amount of literature demonstrates the desire to investigate new sensor

technologies to increase detection potential and expand usability in the biomedical fields.

At least, there exists a mass of literature about various light sources detecting elements by the sensors such as ultraviolet (UV) 19], visible (VIS) [20] and near-infrared (NIR) [21]. Type of light has its own characteristics that vary in the effect to the detection mechanism. The unique properties of each source of light also are important in maximizing sensor performance and improving the detection dynamic. Moreover, the enhancement of the optical substrate properties can either be achieved by their surface modification or facilitation by interactions with target materials, which will lead to significant improvements in the optical performance. These innovations are also important in enhancing the accuracy and usefulness of the sensor in different applications. Regardless of these developments, the existing literature does not provide a proper comparison of the performance of BSA detection by multiple sensing modalities with a single light source and detection system. Precisely, there is minimal comparison which simultaneously compares time response and light intensity and absorbance in cuvette-based, non-bio regulated, and biofunctionalized tapered optical fiber techniques.

This paper optically illustrates the bovine serum albumin concentration optical characteristics of varying concentrations of BSA in various mediums by using three different mediums; cuvettes, non-bios functionalized tapered optical fiber sensors, and bio-functionalized biofunctionalized tapered optical fiber sensors. Though cuvettes are usually used in the biochemical industry, the objective of this comparison is to determine the performance of non-functionalized and biofunctionalized tapered optical fiber sensors, as compared to the conventional cuvette technique. Through the analysis of the results of these sensors, we point out their efficiency in BSA detection.

2. THEORETICAL BACKGROUND

2.1. Electromagnetic Waves

Characteristic of electromagnetic waves are the occurrence of two field directions that are orthogonal, i.e., electric field and magnetic field. These fields extend in space at the same time with perpendicular orientations with regard to each other and the propagation direction of the waves.

2.2. Maxwell's Equations and Wave Equation

The interaction between electric and magnetic fields is governed by Maxwell's equations. In a homogeneous, non-ferromagnetic medium devoid of free charges and currents, these equations can be simplified and combined to yield the wave equation. This equation describes the spatial and temporal evolution of the electric field

$$\frac{\partial^2}{\partial x^2}E(x,t) = \frac{1}{\varepsilon c^2}\frac{\partial^2}{\partial t^2}E(x,t) \quad (1)$$

where
$E(x,t)$ is the electric field at position x and time t;
ε is the dielectric constant;
c is the speed of light in a vacuum.

2.3. Evanescent Wave

The evanescent wave (EW) plays an important role in enhancing the sensor's sensitivity. It appears in the near-surface electromagnetic field when light experiences total internal reflection at the interface between two media with different refractive indexes, such as core and cladding. In a standard optical fiber, this wave is not able to interact with the analyte significantly because it decays exponentially in the cladding. EW intensity *I(z)* decays can be described by :

$$I(z) = I_0 e^{-\alpha z} \quad (2)$$

where
I_0 is the initial intensity of the EW at the surface
α is the decay constant.

Exponentially decaying waves can penetrate the medium, and the penetration depth d_p can be explained by:

$$d_p = \frac{\lambda}{2\pi\left(n_{co}^2 \sin\theta^2 - n_{cl}^2\right)^{\frac{1}{2}}} \quad (3)$$

where
λ is the wavelength of incident light.
θ is the incident angle at the core-medium interface.

The sensor was tapered to enhance the strength of the EW in the cladding area. Its diameter was reduced to less than its core diameter, allowing light to pass through the analyte at the sensing area. In the tapered region, Point Z represents the location between the core and cladding layers where the incident angle is produced, as illustrated in Figure 1. The incident angle $\theta_i(z)$ is given by :

$$\theta_i(z) = \frac{\pi}{2} - \beta_T - \alpha_z \quad (4)$$

where β_T and α_z correspond to the taper and launch angle respectively. The taper angle (β_T) can be explained as follows:

$$\beta_T = \tan^{-1}\left(\frac{R_0 - R_L}{L}\right) \quad (5)$$

where R_0, R_L and L are the initial radius, final taper radius, and tapered region length, respectively.

The taper profile influences the launch angle α_z for a tapered structure. In the specific case of a linear taper geometry, the relationship between these parameters can be described by the following equation:

$$\alpha_z = \sin^{-1}\left[\frac{\sin\alpha_0}{z(R_L/R_0 - 1)/L + 1}\right] \quad (6)$$

Here, z represents the height and spans the range from R_L to R_0, while α_0 denotes the initial angle of the guided ray at

the fiber's input end. However, for a parabolic profile, the relationship varies. The α_z is characterized as follows:

$$\alpha_z = \sin^{-1}\left[\frac{\sin\alpha_0}{z(R_L/R_0-1)/L+1}\right] \quad (7)$$

For an exponentially tapered fiber, the relationship is described as follows:

$$\alpha_z = \sin^{-1}\left[\frac{\sin\alpha_0}{z(1-R_L/R_0)\left[exp(-z/L)-\left(\frac{z}{L}\right)\exp(-1)\right]+R_L/R_0}\right] \quad (8)$$

The equations show that the angle z in taper geometry determines the penetration depth of the evanescent waves, which in turn affects the sensor sensitivity.

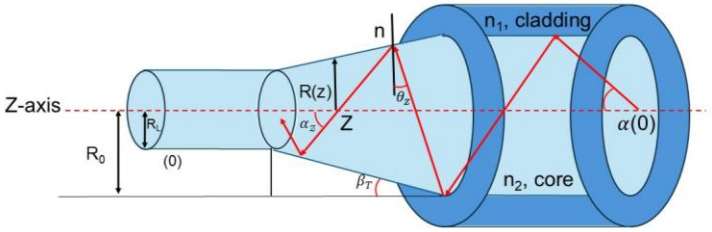

Figure 1. Light transmission in tapered optical fiber BSA measurement experimental setup using cuvette.

3. METHODOLOGY

There were three experimental designs used in investigations in this study, that is, a cuvette, a non-biofunctionalized tapered optical fiber, and a biofunctionalized tapered optical fiber.

3.1. Sample Preparation

3.1.1. BSA Solution Preparation

BSA solutions were made in this study with the concentration of 125 mg/dL through 31.25 mg/dL. An analytical balance was used to weigh an exact amount of 62.5 mg to get BSA pellets. About 40-45 mL of deionized (DI) water was incorporated into a beaker, over which the pellets of BSA were incorporated slowly. The blend was stirred, and the pellets of BSA dissolved in the DI water. A volumetric flask was then used to transfer the obtained BSA solution into the flask, and a beaker was washed with more DI water to completely transfer the solution into the flask. The volumetric flask was filled with DI water up to the 50 mL mark. The volumetric flask was then flipped several times to ascertain that the solution was well mixed.

3.1.2. Sodium Hydroxide Solution Preparation

Sodium hydroxide that is provided by R&M Chemical company is used in the hydroxylation process on the sensing surface. An exact weight of 0.4 g of NaOH was weighed on a weighing balance and dissolved in 100 mL of deionized water

.

3.1.3. 3-aminopropyltriethoxysilane (APTES) Solution Preparation

An experimental solution of 3-aminopropyltriethoxysilane (APTES) was made up in 2% (v/v) of 98 percent pure solution. These were measured with a micropipette; 1.02 mL of the 98% solution was transferred into a beaker. Deionized water was added subsequently to the beaker until the lessening volume reached 50 mL. The mixture was swirled continuously to make the APTES uniformly diluted to the desired concentration of 2% of 1.

3.1.4. Glutaraldehyde Solution Preparation

A 2 mL of the 50 percent glutaraldehyde solution (Sigma-Aldrich) was taken using a micropipette and poured in a beaker with 50mL of deionized water. Every precaution was followed, and the mixture was completely stirred to get it homogenized.

3.1.5. Tapered Optical Fiber Fabrication

The heat-pull mechanism became a tool for making tapered fiber optic sensors with a Vytran machine (GPX-3400). The technique was used because it has the ability to produce tapered fibers in a uniform and accurate way [22]. The parameters used to construct this sensor come as a result of an optimized design, which is highly optimized due to the widespread trial and error by the earlier researchers [23].. At the first stage, the cladding layer of the central part of the optical fiber was removed. The resulting prepared fiber was then loaded in the filament area of the machine, with each end being placed in the fiber holders. The fiber holders were forced to cut off two tapered ends on each side of a narrower middle area during the heating process with a motor. The core area acts as a sensing one of tapered optical fiber sensors.

3.2. Experimental Setup

3.2.1. Conventional Cuvette Method

The experiment design as shown in Figure 2 involved the following: A DT-2-GS light source was connected to the cuvette holder with the help of an SMA 905 multimode optical fiber cable; another component was attached to the Flame Ocean Optic spectrometer with the assistance of one more SMA 905 multimode optical fiber cable. In the course of the experiment, a 3.5 mL quartz cuvette was used. Three

BSA solutions were diluted to different concentrations of between 125 mg/dL and 31.25mg/dl and then measured with the cuvette.

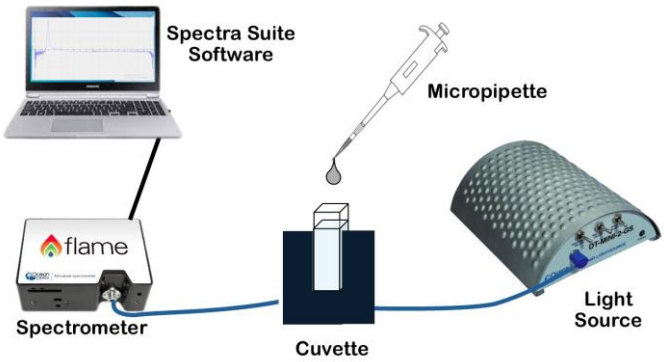

Figure 2. The experimental setup for measurement of BSA using a cuvette.

3.2.2. Non-Bio Functionalized Tapered Optical Fiber

The second experimental method, as shown in Figure 3 was also similar to the first experiment except the cuvette and cuvette holder were substituted with non-bio functionalized tapered fiber sensors and sensor holder respectively. The tapered optical fiber employed in this system had a waist length of 10 mm, a waist diameter of 10 mu and an upper taper length of 10 mm and the lower taper length of 10 mm. The method entailed application of the Dip-Coat method in which the sensor area was coated with BSA solutions to the point whereby the immersed part of the sensor had fully immersed in the solution.

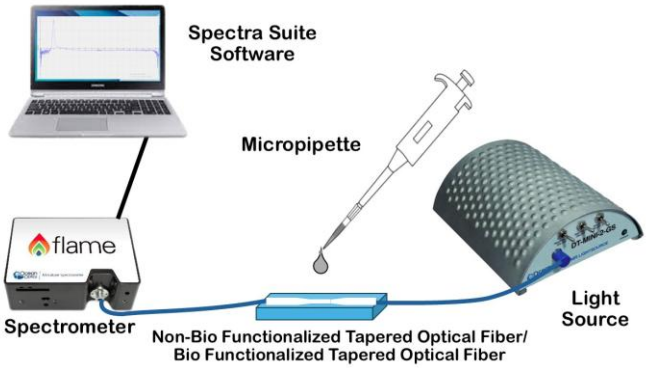

Figure 3. Experimental setup of BSA measurement using non- bio functionalized tapered optical fiber/ bio functionalized tapered optical fiber.

3.2.3. Biofunctionalized Tapered Optical Fiber

The biofunctionalization of the sensor was adopted to improve the adhesion of organic analytes to the sensing surface in three primary steps, which were hydroxylation, salinization, and aldehyde treatment. The procedures and the formulations of the materials applied in the experimental works carried out in the study are founded on the methodologies developed in the previous studies [24]. The purpose of the hydroxylation was to add to the surface of the sensor more of the hydroxyl (–OH) groups. In order to do so 120 µL of the 0.1 M sodium hydroxide (NaOH) was placed on the optical fiber sensor and allowed to dry one hour.

The biofunctionalization of the sensor was implemented to enhance the adhesion of organic analytes to the sensing surface, comprising three main steps: hydroxylation, salinization, and aldehyde treatment. The experimental procedures and material formulations utilized in this study are based on methodologies established in prior research. The hydroxylation process aimed to increase the density of hydroxyl (–OH) groups on the sensor's surface. To achieve this, 120 µL of 0.1 M sodium hydroxide (NaOH) was applied to the optical fiber sensor, which was then left to soak for one hour.

The salinization process was then done to transform the hydroxyl groups into aminopropyl groups. This was done by incubating the sensor with 3-aminopropyltriethoxysilane (APTES) 2 per cent (v/v) solution, in one hour. The last step was aldehyde treating, which was a bifunctional linker, and it helped in the attachment of BSA to sensor. Throughout this step, aldehyde molecules that are attached to the free amino groups of the silane-treated sensor formed covalent amide bonds whereas other aldehyde molecules reacted with the amino groups found in BSA.

The success of every functionalization step was followed by counting the optical absorption rate using the spectrometer.

The sensor was dried at room temperature after biofunctionalization had been completed in three washes with deionized water. The sensor was arranged as in Figure 2. The method employed in the experiment was dip coating, in which a solution of BSA was gently patted on the area that was to be detected. Three hours of air drying was then permitted to the sensing region in order to permit a successful binding of the BSA molecules and at the same time provide stability.

4. DATA COLLECTION AND ANALYSIS

4.1. Time Responses

In this research, the response times of three methods were recorded in a systematic manner to be compared in different methods, as indicated in Figure 4. Figure 4 (a) indicates that the response time of absorption measurements with a cuvette had the initial spike of 3.5 optical density (OD) corresponding to instability in the first 70 seconds, which, probably, can be attributed to the introduction of the BSA sample. The system then stabilized at 140 seconds with an OD value of 0.68.

The subsequent graph, Figure 4(b), indicates that the graph gradually increased up to 0.28 OD in the next 50 seconds, after which the absorption started to decrease to 0.041 OD, with occasional variations. The stabilization period was about 330 seconds, after which a final absorption value of 0.036 OD was recorded. The initial spikes in the cuvette and optical fiber sensor techniques are explained by the existence of interactions between the BSA molecules and the detection media.

The first peaks in Figures 4(a) and 4(b) at the early stages of absorbance measurements can probably be explained by multiple temporary effects. These are mixing effects at the beginning, whereby the BSA molecules might not be evenly dispersed in the medium and as such, cause short-term concentration gradients that act on the light absorption. Also, due to the development of microbubbles (or trapping air) during sample loading, localized scattering, and refractive index can be introduced to the optical signal, consequently distorting optical signal. Solution settling can also play a role in that the protein molecules take time to stabilize in the detection volume, and this results in variations in absorbance as the system changes to equilibrium. Besides, interactions at an early phase between BSA molecules and the detection surface can cause either temporary refractive index changes or incomplete binding conditions that can occur when the inner wall of the cuvette or the tapered optical fiber interface is used. These together cause temporary peaks and dales in the absorbance signal before the steady-state conditioning is attained.

Also, Figure 4(c) shows a steep fall in the value of absorption to -0.038 OD, after which the value becomes gradual in its fall up to 800 seconds. The primary decrease is attributed to the binding of the BSA molecules with the functionalized surface that entailed the release of energy, leading to the negative values of absorption.

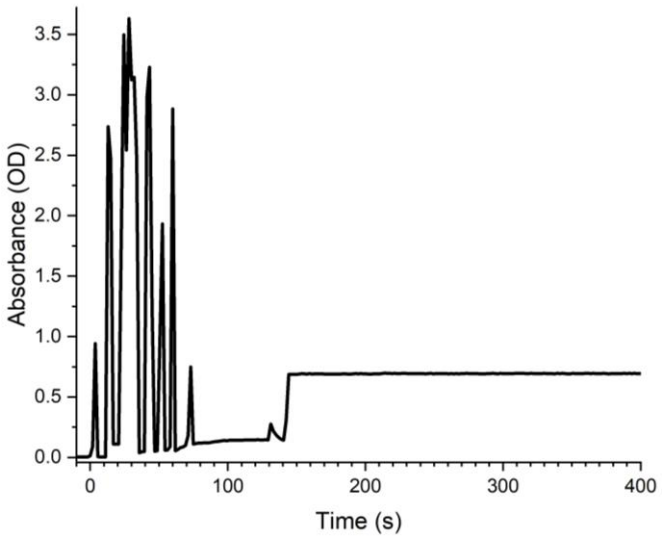

(a)

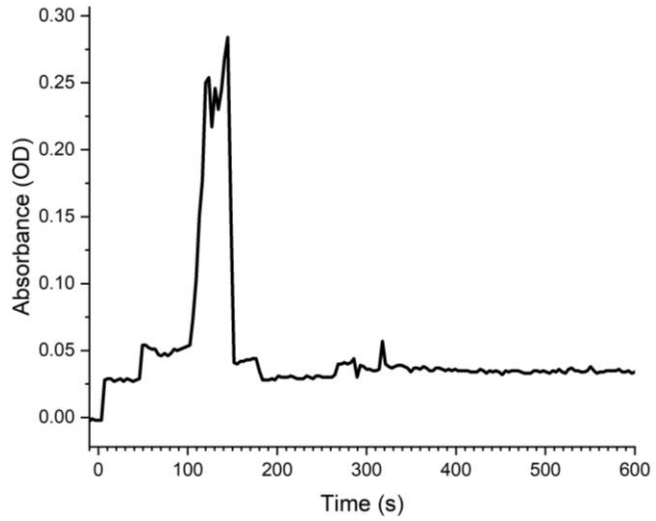

(b)

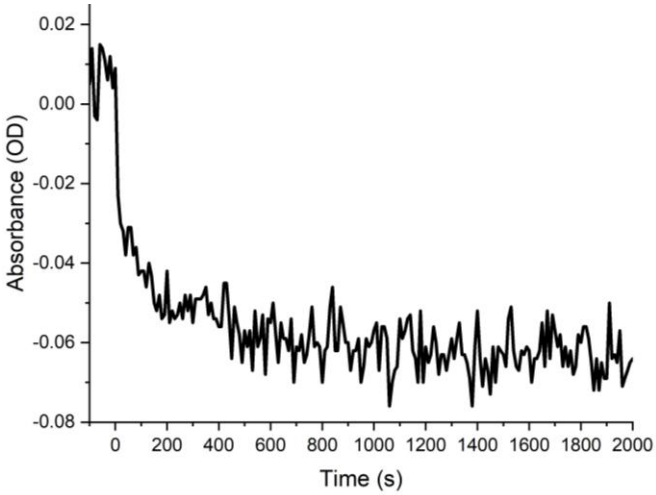

(c)

Figure 4. Response time to the absorbance level of BSA with (a) cuvette, (b) tapered optical fiber, and (c) biofunctionalized tapered optical fiber.

4.2. Intensity Analysis

The analysis that follows is concerned with the measurements of light intensity expressed in counts, which are representative numbers that show the amount of light that is detected by the spectrometer at certain wavelengths. In Figure 5 (a) the penetration of light through the BSA in a cuvette was observed at three concentrations. The values demonstrate notable peaks at 320 nm, 500 nm, and 585 nm wavelengths with the values of the intensity of 2,500 to 45,000 counts. The concentration with the highest intensity (BSA 125 mg/dL) at 320 nm indicates that having the highest concentration has a greater intensity of color absorption.

There is a significant difference in the intensity of light among the three concentrations in the values between 275 and 285 nm, which is located in the UV spectrum. This difference can probably be explained by the fact that when concentrations are high, lighter and BSA moles interact, especially with the aromatic amino acids tryptophan, tyrosine, and phenylalanine, which are the strongest absorbers in the UV spectrum. The more these amino acids absorb, the less light is passed through the solution. Beyond this wavelength range, the variations in the concentrations would not be significant.

Conversely, in cases where the light intensity is determined by a tapered optical fiber biosensor, a specific spectrum is produced, and the intensity value ranges between 2,500 and 14,000 counts, as illustrated in Figure 5 (b). Installation of tapered optical fibers as biosensors leads to low intensity of the light received by the spectrometer. The process of this reduction is because light passes through the tapered fiber, some of which will leave the core and the cladding and interact with the sensor surface, with the rest of the process going on in the core to the spectrometer. The spectrum shows the primary peak at about 582 nm as well as the secondary peak at 603 nm. In line with the cuvette measurements, an increase in concentrations of BSA is associated with a decrease in the readings on the light intensity.

Figure 5(c) also illustrates the variation in intensity of light at the sensor surface prior to and after applying BSA on sensor surface. In the range of wavelengths between 362

nm and 725 nm, a lot of difference is witnessed in the intake of the light at higher BSA concentrations compared to lower concentrations. This disparity can be explained by the light that leaves the core and the cladding first trying to interact with the bio-functionalized biofunctionalized optical surface, followed by the BSA molecules that bind to the bio-functionalized biofunctionalized tapered optical fiber sensor surface. Subsequently, more light interacts with the surface than was the case in the original state. And beyond this wavelength region, the variation in light intensity amongst concentrations of the BSA is also evidenced, but it is not as strong.

4.3. Absorbance Analysis

The following analysis is an absorbance analysis. Figure 6(a) demonstrates that the peaks of absorbance of BSA solutions at different concentrations have different values. In the absorbance spectrum at 229 nm and at 277 nm, there is a distinguishable peak. The peak value at 229 nm is attributed to the π-pi transition of the peptide backbone whereas the peak at 277 nm is attributed by the absorption of aromatic amino acids like tryptophan, tyrosine, and phenylalanine [25]. It is worth noting that, none of the spectra have a large absorbance in the visible and NIR.

The difference between the absorbance properties in the use of non-bio functionalized tapered fiber optic sensor and traditional cuvettes evidence that the absorbance is less than 5 percent in the latter, as shown in Figure 6(b). This is decreased on the basis of reduced light collection capability of the fiber optic system since only part of the light guided through the system is permitted to exchange through the EW. In contrast to traditional cuvettes, the full optical path is in direct contact with the sample non-bio functionalized tapered optical fiber that makes use of the evanescent field. An electromagnetic field that causes exponential (decreases) attenuation and spreads outward through the fiber wrapping into the adjacent medium. Part of the light and analyte molecules can interact in this field at the surface. The Beer Lambert law states that the absorbance (A) is proportional to the concentration (C), path length (l), and the molar extinction coefficient (ε) and is given as

$$A = \varepsilon C l$$

In the bearer of non-bio functionalized tapered optical fibers the effective path essentially relies on the depth of the penetration of the evanescent wave, which is determined by the wavelength, the difference in refractive indices, and the form of the taper. Consequently, it consequently leads to the evanescent wave intensity modulating absorbance which decays exponentially near the surface of the fiber. The lower EW intensity or decreased penetration depth results in lower values of effective absorbance as can be seen in this figure.

The absorbance maxima at the wavelength of 340 visible as the main result of lysine charge transfer transitions applies at wavelengths even longer [26].. The decreasing pattern of absorbance at longer wavelengths is in agreement with a falling pattern of molar extinction coefficient. Still, the continuum absorbance increases between 647 and 750 nm that can be attributed to weak vibrational overtone interactions.

Figure 6 (c) indicates that the greatest absorbance is obtained in the highest concentration of BSA in nearly all spectra below 915 nm indicating that successful immobilization of BSA has occurred in the functionalized surface. Improved surface binding with the sensor surface results in amplified evanescent field-immobilized BSA molecules interaction. Whereas in the visible range (400-700 nm), the monitoring of the absorbance remains quite stable, this shows the stability and reliability of the sensor used to identify the presence of BSA. There is also a weak increase in absorbance in the NIR region (650 -1000 nm), which can probably be attributed to the vibrational overtones and the combination bands associated with BSA. The act of reinforcing the fact that, the high evanescent field interactions responsible in increasing surface functionalization contribute directly to surface increment of effective optical path length and increased absorbance responses, therefore, upholding the Beer Lambert relationship naturally, in the evanescent wave-based sensing context.

The realized difference between the unimportant change between the intensity variation with BSA concentration in Figure 5(b) and the distinct absorbance rise in Figure 6(b) may be explained by the very nature of light coupling efficiency and mode confinement in tapered optical fiber sensor. Though an inverse relationship exists in the Beer Lambert law between absorbance and the intensity of the transmitted light, the relationship presumes a monochromatic and constant path length in the sample. In tapered optical fibers the portion of the propagated light which appears as an evanescent wave is transferred to the external media and the rest of the light is delivered to the core of the fiber but with little interaction. Consequently, the observed changes of intensity might be subtle because the fraction of light that is interacting with an analyte is not large.

Also, modal dispersion, bending losses on the fibers, and imperfect alignment on the dip-coating process can be sources of variance and quashable variations on actual raw values of intensity. Conversely, the absorbance spectrum in Figure 6(b) was obtained using processed data, which considers both baseline corrections and spectral integration which is more sensitive to sensitive changes of the molecular interaction and concentration. Thus, whereas raw intensity changes cannot be perceived as important in Figure 5(b), the calculation of absorbance destroys the diffusion of concentration-dependent tendencies which is also in line with the predicted optical behavior.

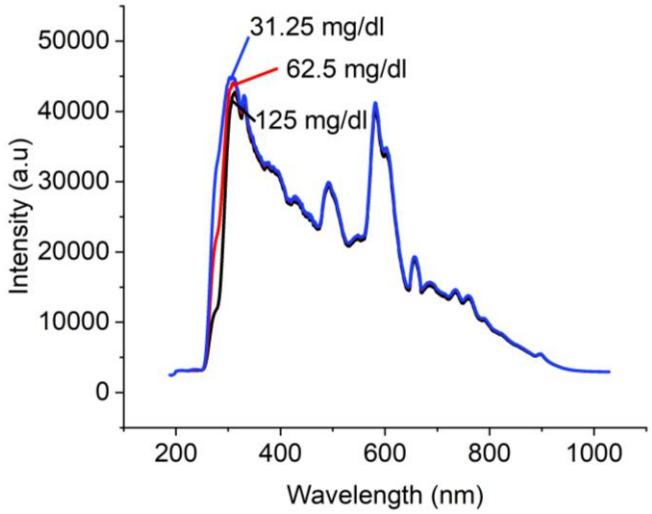

(a)

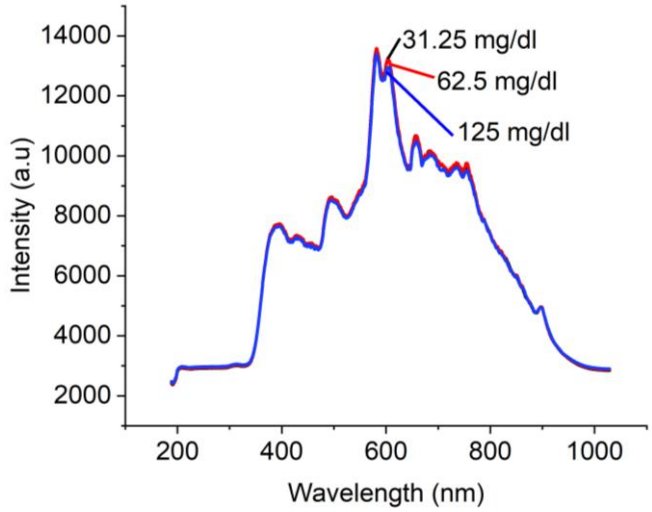

(b)

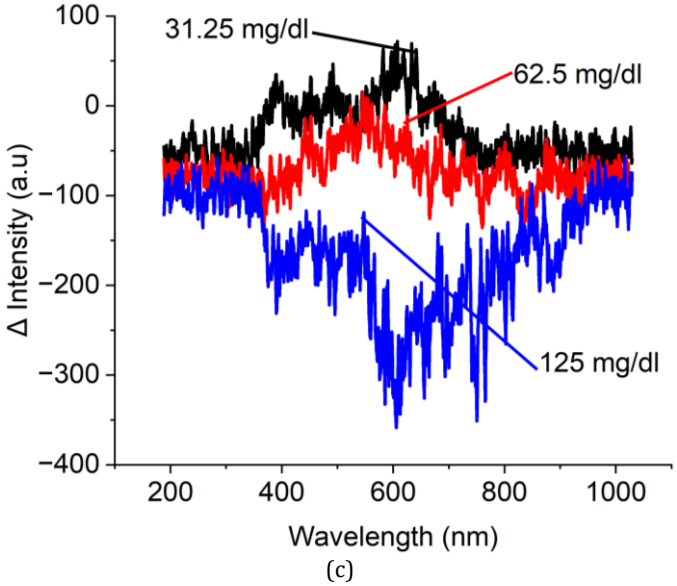

(c)

Figure 5. Value of light intensity at the UV-VIS-NIR wavelength with (a) cuvette; (b) tapered optical fiber and (c) changes light intensity value at the UV-VIS-NIR wavelength using bio functionalized tapered optical fiber.

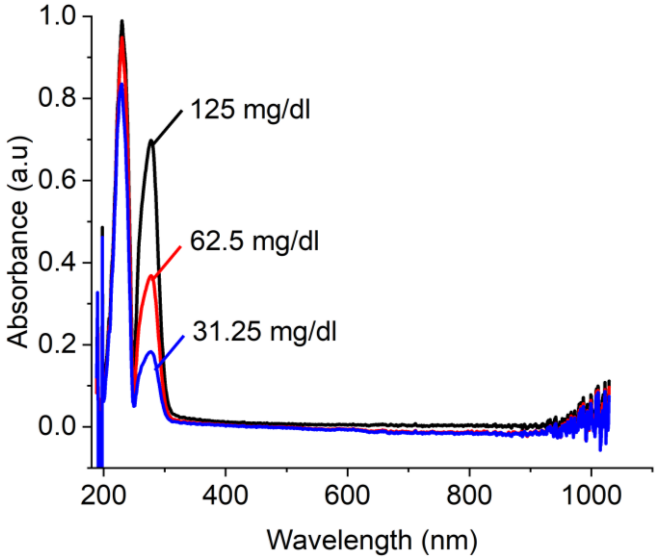

(a)

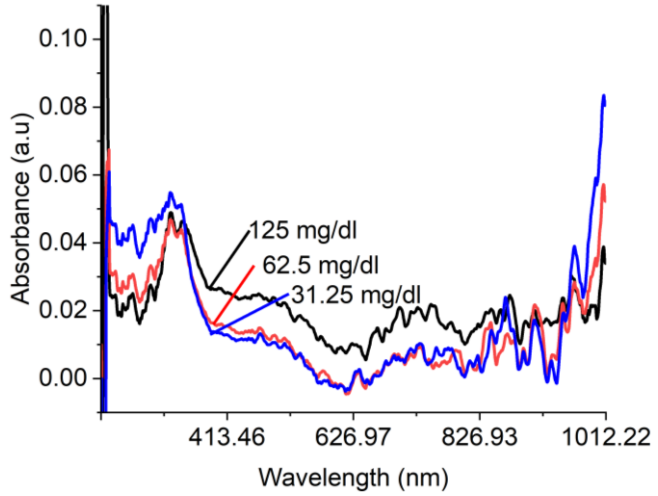

(b)

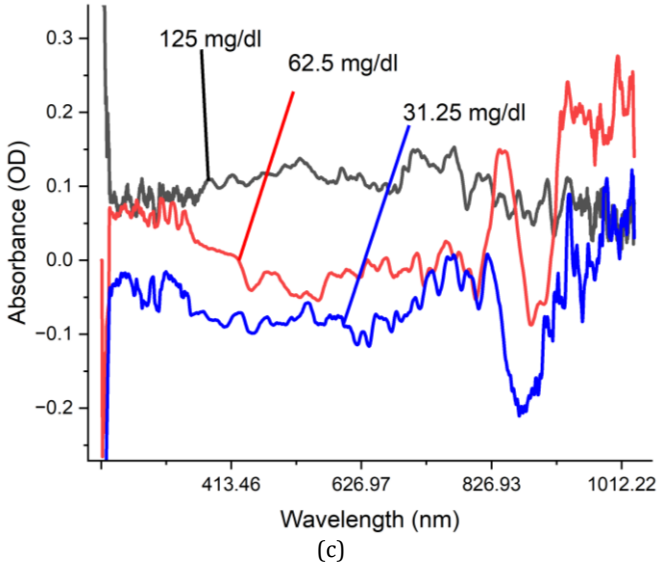

(c)

Figure 6. The absorbance value at UV-VIS-NIR wavelength with (a) cuvette; (b) non- bio functionalized tapered optical fiber and (c) bio functionalized tapered optical fiber.

5. DISCUSSION AND RESULTS

5.1. Comparative Analysis of Various BSA Detection

Table 1 gives a brief overview of the main results in the spectrum intensity and absorbance, giving a solid idea of the crucial points of the data, which are the basis of the analysis of this study.

Table 1 Comparative Analysis of Various BSA Detection

Range	Cuvette	Non-Bio Fuctionalizedtapered Optical Fiber	Bio Functionalized Tapered Optical Fiber
Intensity			
UV 189-380 nm	• Low intensity • Highest peak: 236 nn	• 189-220nm: rapid increment • 220-340 nm: Rises gradually	• Noise • Highest concentrations = lowest intensity
Visible (380– 750 nm)	• 350-750 nm: gradually decreases • Highest peak: 582 nm	• 380-750 nm: rises steadily • Highest peak: 582 nm and-603 nm	• Distinct profile spectrum • Changes are greatest at the highest concentration.
NIR (750 -1029 nm)	• 750 – 1029 nm: gradually decreases	750 – 1029 nm: gradually decreases	• Lower concentration: maintained • Higher concentration: progressive climb
Absorbance			
UV (189 nm – 380 nm)	• High absorbance: 229 and 277 nm	• High absorbance: 340 nm • Inverse relationship between absorbance and concentration • An inverse relationship between absorbance and concentration below wavelength 340 nm. • High noise.	• Highest concentration: low gap • Lowest concentration: high gap • High noise.
Visible (380 nm – 750 nm)	No absorbance detected	• 380-647 nm: absorbance spectrum decrease. • 648-750 nm: absorbance spectrum increase. • High noise.	• Higher gap absorbance between 125 mg/dL and 62.5 mg/dL concentration. • Low gap absorbance between 62.5 mg/dL and 31.25 mg/dL concentration.
NIR (750 nm -1029 nm)	No absorbance detected	• The absorbance increased towards the longer wavelength. • An inverse relationship with concentration. • High noise	• The highest absorbance is 62.5 mg/dL concentration, followed by 125 mg/dL and 31.25 mg/dL concentrations. • High noise

5.2. Calibration Curve

The size of the light intensity and the data of the absorption spectrum play an important role in the finding of an analyte. In the current study, the sensitivity was measured by the evaluation of the calibration curve used in the UV band. The calibration curve of the total light intensity of non-bio functionalized tapered optical fiber, bio functionalized tapered optical fiber, and cuvette medium is shown in figure 7 (a) (i) -(iii). In the given experiment the sensitivity value is negative since the decrease in the noticed light by the spectrometer is proportional to the increase in the BSA content. The cuvettes presented high values of sensitivity and then came bio functionalized tapered optical fiber and non- bio functionalized tapered optical fiber. The Sensitivity of non-bio functionalized tapered optical fiber was 0.9996S/min which was 99.96S/min lower when compared to cuvette medium. The functionalized version, however, showed a 207.1 percentage height in the sensitivity with the values moving to -1.99477 as compared to -0.64962. This improvement was given by determining the percentage change in the sensitivity of BFTOF compared to NBTOF.

$$Sensitivity\ Increase\ (\%) = \left(\frac{-1.9947 - (-0.64962)}{|-0.64962|}\right) \times 100$$

$$\left(\frac{-1.34508}{-0.64962}\right) \times 100 \approx 207.1$$

The bio functionalized tapered sensitivity value is merely 0.962% of the sensitivity seen on the cuvette because of a significant disparity in the intensity levels employed in the two scenarios.

$$Relative\ Sensitivity\ (\%) = \left(\frac{-1.9947}{-207.26403}\right) \times 100 \approx 0.962$$

Similar sensitivity pattern in the calibration curve of absorbance in Figure 7 (b) I-III indicates the existence of critical differences in the detection efficacy. It is important to note that the cuvette has the optimum sensitivity of 0.00546 which is very high as compared to the biofunctionalized and non-biofunctionalized tapered optical fibers which have sensitivities of 0.00195 and 1.2228e-4 respectively. The non-bio functionalized tapered optical fiber sensitivity has decreased 97.76 percent of 0.00546 to 1.22286e-4 relative to the cuvette medium which is similar to the sensibility of the light intensity. The sensitivity of tapered optical fiber is significantly improved by biofunctionalization by a very impressive percentage of 1494.72. This high enhancement highlights the possibility of biofunctionalized tapered fibers in the capacity of precision sensing, which makes them an attractive alternative in the area. This is on the basis of the relative growth of BFTOF over the growth of NBTOF; which was calculated as below:

$$Sensitivity\ Increase\ (\%) = \left(\frac{0.00195 - 0.000122286}{0.000122286}\right) \times 100 \approx 1494.72$$

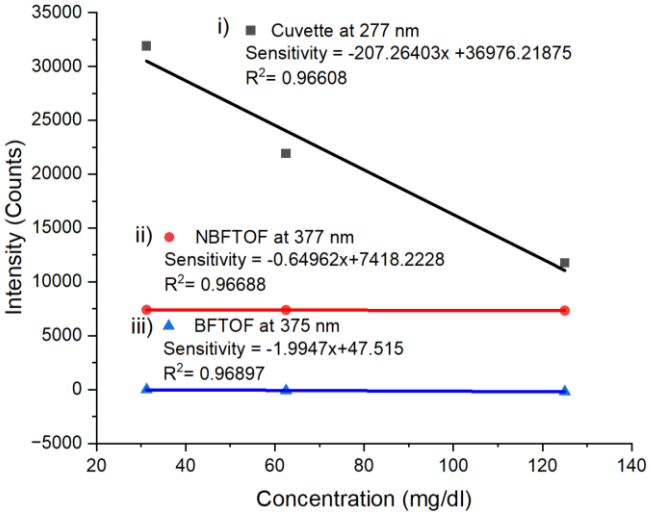

(a)

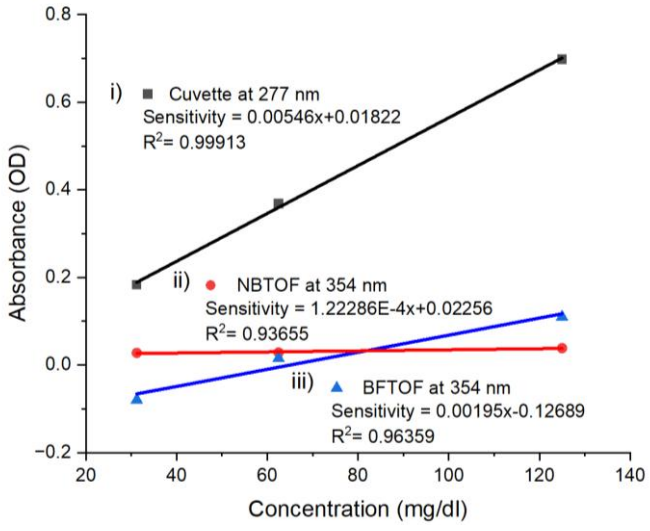

(b)

Figure 7. Calibration curve for cuvette, tapered optical fiber and biofunctionalized tapered optical fiber using (a) intensity and (b) absorbance measurement.

Table 2 provides a comparative analysis of BSA detection of four past studies based on optical methodology. Photothermal lens has been shown to be a better method in terms of sensitivity when compared to this experiment, but it uses a very large sample, 1.4 mL. Conversely, it is in this paper that 120 µL of analyte can be successfully detected using a bio-functionalized biofunctionalized tapered optical fiber sensor to detect BSA.

Table 2 The reported BSA detection by optical sensor

No	Optical Substrate	Detection Method	Detection Range	Sensitivity	Ref
1	Hollow-core microstructured optical waveguides	Transmission	1000, 2000, 4000, 6000 mg/dl	6.44 mL/mg	[27]
2	quartz semi-microcell	Photothermal lens signal	0.05-7.5 mg/dl	0.0212 a.u./(µg/ml)	[28]
3	Cuvette	Absorbance	1,2,3,4,5,7.5, 10, 12.5, 15, 20, 25 and 50 nM	-0.11835 (OD/nm)	[29]
4	Micro-taped-long-period fiber grating	Wavelength shift	40, 80, 120, 160, 200 mg/dl	0.043 mg/mL	[30]
5	Bio functionalized tapered optical fiber	Intensity	125 mg/dl, 62.5 mg/dl & 31.25 mg/dl	-1.9947 a.u/(mg/dl)	This work
6		Absorbance	125 mg/dl, 62.5 mg/dl & 31.25 mg/dl	0.00195 a.u/(mg/dl)	

6. CONCLUSION

Finally, the paper presents an in-depth analysis of the BSA detection based on different sensing modalities and shows the benefits and drawbacks of each of the approaches. The findings prove that although cuvettes would give better performance in terms of high volume and should be used to analyze the performance of absorbance value, which provides the greatest sensitivity at the cost of topped optical fibers, the biofunctionalization would give the indicated result on tapered optical fibers of a 1494% increase in sensitivity and a 206% increase in intensity, respectively. This is, yet, not as high as the cuvettes, but it shows the potential of the biofunctionalized tapered fibers to make a significant change in the precision sensors. The time response study is valuable in providing important understanding of the interactions between the BSA molecules and the sensing surfaces, and biofunctionalized fibers have the potential to yield more steady and stable measurements in terms of time. The intensity and absorbance tests also help in the confirmation of the usefulness of these fibers in the signaling of BSA, especially in the UV and visible spectrum, which traditional cuvettes might be deficient in. Together, these results make biofunctionalized tapered optical fibers a promising alternative in biosensing and the possible revolutionization of detection schemes in biomedical and environmental biosensing. It is important to note that the high improvements in sensitivity and stability would lead to the increased body of knowledge and future innovations in fiber optic sensor design.

ACKNOWLEDGEMENTS

This research was funded by Universiti Kebangsaan Malaysia through INISIATIF BELANJAWAN 2025: AI ENHANCEMENT, Malaysia, under the grant WARISAN-2025-023.

REFERENCES

[1] M. Ruzicka, L. Jabloncik, P. Dejdar, A. Tomasov, V. Spurny, and P. Munster, "Classification of Events Violating the Safety of Physical Layers in Fiber-Optic Network Infrastructures," *Sensors*, vol. 22, no. 23, 2022, doi: 10.3390/s22239515.

[2] X. Guo *et al.*, "A High-Precision Transfer of Time and RF Frequency via the Fiber-Optic Link Based on Secure Encryption," *Appl. Sci.*, vol. 12, no. 13, 2022, doi: 10.3390/app12136643.

[3] L. Liu, Y. Liu, and X. Gao, "Flexible Ultra-Wide Electro-Optic Frequency Combs for a High-Capacity Tunable 5G+ Millimeter-Wave Frequency Synthesizer Li," *Appl. Sci.*, vol. 22, no. 11, p. 10742, 2021.

[4] D. Venu, A. V. R. Mayuri, S. Neelakandan, G. L. N. Murthy, N. Arulkumar, and N. Shelke, "An efficient low complexity compression based optimal homomorphic encryption for secure fiber optic communication," *Optik (Stuttg).*, vol. 252, no. December 2021, p. 168545, 2022, doi: 10.1016/j.ijleo.2021.168545.

[5] J. Zhou *et al.*, "Miniature non-contact photoacoustic probe based on fiber-optic photoacoustic remote sensing microscopy," *Opt. Lett.*, vol. 46, no. 22, p. 5767, 2021, doi: 10.1364/ol.444889.

[6] H. Liu *et al.*, "Uav-borne hyperspectral imaging remote sensing system based on acousto-optic tunable filter for water quality monitoring," *Remote Sens.*, vol. 13, no. 20, 2021, doi: 10.3390/rs13204069.

[7] Y. Kitahama, M. Egawa, P. K. Dwivedi, W. Yang, and K. Goda, "An emerging tool in healthcare: wearable surface-enhanced Raman Spectroscopy," *JPhys Photonics*, vol. 6, no. 2, pp. 0–16, 2024, doi: 10.1088/2515-7647/ad38f6.

[8] W. Lyu, S. Chen, F. Tan, and C. Yu, "Vital Signs Monitoring Based on Interferometric Fiber Optic Sensors," *Photonics*, vol. 9, no. 2, 2022, doi: 10.3390/photonics9020050.

[9] Z. Zhu, L. Liu, Z. Liu, Y. Zhang, and Y. Zhang, "Surface-plasmon-resonance-based optical-fiber temperature sensor with high sensitivity and high figure of merit," *Opt. Lett.*, vol. 42, no. 15, pp. 2948–2951, Aug. 2017, doi: 10.1364/OL.42.002948.

[10] H. Liu *et al.*, "High-Temperature Fiber-Optic Fabry–Perot Vibration Sensor Based on Single-Crystal Sapphire," *Sensors*, vol. 23, no. 10, 2023, doi: 10.3390/s23104952.

[11] S. K. Al-Hayali, A. M. Salman, and A. Hadi Al-Janabi, "Effect of hygroscopic polymer-coatings on the performance of relative humidity sensor based on macro-bend single-mode fiber," *Opt. Fiber Technol.*, vol. 62, no. February, p. 102460, 2021, doi: 10.1016/j.yofte.2021.102460.

[12] Y. Deng *et al.*, "Fiber optic coupled surface plasmon resonance sensor based Ag-TiO2 films for hydrogen detection," *Opt. Fiber Technol.*, vol. 65, no. February, 2021, doi: 10.1016/j.yofte.2021.102616.

[13] J. L. C. Perez *et al.*, "Fiber optic sensors: A review for glucose measurement," *Biosensors*, vol. 11, no. 3, 2021, doi: 10.3390/bios11030061.

[14] G. Besselink *et al.*, "Asymmetric Mach–Zehnder Interferometric Biosensing for Quantitative and Sensitive Multiplex Detection of Anti-SARS-CoV-2 Antibodies in Human Plasma," *Biosensors*, vol. 12, no. 8, 2022, doi: 10.3390/bios12080553.

[15] M. Sahay *et al.*, "Aetiology, practice patterns and burden of end-stage kidney disease in South Asia and South-East Asia: A questionnaire-based survey.," *Nephrology (Carlton).*, vol. 26, no. 2, pp. 142–152, Feb. 2021, doi: 10.1111/nep.13825.

[16] H. M. Teeuw, H. B. Amoakoh, C. A. Ellis, K. Lindsley, and J. L. Browne, "Diagnostic accuracy of urine dipstick tests for proteinuria in pregnant women suspected of preeclampsia: A systematic review and meta-analysis," *Pregnancy Hypertens.*, vol. 27, no. December 2021, pp. 123–130, 2022, doi: 10.1016/j.preghy.2021.12.015.

[17] J. R. Mejia *et al.*, "Diagnostic accuracy of urine dipstick testing for albumin-to-creatinine ratio and albuminuria: A systematic review and meta-analysis," *Heliyon*, vol. 7, no. 11, 2021, doi: 10.1016/j.heliyon.2021.e08253.

[18] R. Thakur, P. Maheshwari, S. K. Datta, S. K. Dubey, and C. Shakher, "Machine Learning-Based Rapid Diagnostic-Test Reader for Albuminuria Using Smartphone," *IEEE Sens. J.*, vol. 21, no. 13, pp. 14011–14026, 2021, doi: 10.1109/JSEN.2020.3034904.

[19] B. D. Frank, M. Antonietti, P. Giusto, and L. Zeininger, "Photocharging of Carbon Nitride Thin Films for Controllable Manipulation of Droplet Force Gradient Sensors," *J. Am. Chem. Soc.*, pp. 0–5, 2023, doi: 10.1021/jacs.3c09084.

[20] G. Wang, X. Xu, J. Ren, P. Xie, and R. Li, "Sensing performance enhancement of plasmonic waveguide sensor using a bimodal strategy with digital Gaussian filter," *Chemom. Intell. Lab. Syst.*, vol. 245, no. October 2023, p. 105069, 2024, doi: 10.1016/j.chemolab.2024.105069.

[21] Y. Zhao, C. Li, Z. T. Lin, Y. Wang, R. Tong, and L. Cai, "Plug-and-Play Fabry-Perot interferometric biosensor with Vernier effect for label-free detection of bovine serum albumin," *Sensors Actuators B Chem.*, vol. 416, no. January, p. 135999, 2024, doi: 10.1016/j.snb.2024.135999.

[22] N. Burham *et al.*, "Effect of Coated Tungsten Disulfide (WS2) on Tapered Optical Fibre for Urea Detection," *J. Adv. Res. Appl. Sci. Eng. Technol.*, vol. 39, no. 2, pp. 181–190, 2024, doi: 10.37934/araset.39.2.181190.

[23] M. A. Mustapa, M. H. Abu Bakar, Y. Mustapha Kamil, A. Syahir, and M. A. Mahdi, "Bio-Functionalized Tapered Multimode Fiber Coated with Dengue Virus NS1 Glycoprotein for Label Free Detection of Anti-Dengue Virus NS1 IgG Antibody," *IEEE Sens. J.*, vol. 18, no. 10, pp. 4066–4072, 2018, doi: 10.1109/JSEN.2018.2813385.

[24] N. H. Zainuddin *et al.*, "Enhanced detection sensitivity of Leptospira DNA using a post-deposition annealed carbon quantum dots integrated tapered optical fiber biosensor," *Opt. Mater. (Amst).*, vol. 141, no. March, p. 113926, 2023, doi: 10.1016/j.optmat.2023.113926.

[25] X. Zhao, R. Liu, Z. Chi, Y. Teng, and P. Qin, "New insights into the behavior of bovine serum albumin adsorbed onto carbon nanotubes: Comprehensive spectroscopic studies," *J. Phys. Chem. B*, vol. 114, no. 16, pp. 5625–5631, 2010, doi: 10.1021/jp100903x.

[26] S. Prasad *et al.*, "Near UV-Visible electronic absorption originating from charged amino acids in a monomeric protein," *Chem. Sci.*, vol. 8, no. 8, pp. 5416–5433, 2017, doi: 10.1039/c7sc00880e.

[27] A. Merdalimova *et al.*, "Two-in-one sensor of refractive index and Raman scattering using hollow–core microstructured optical waveguides for colloid characterization," *Colloids Surfaces B Biointerfaces*, vol. 234, no. December 2023, p. 113705, 2024, doi: 10.1016/j.colsurfb.2023.113705.

[28] N. A. Behnaz Abbasgholi, N. Shokoufi, and S. Nouri Hajibaba, "Bovine serum albumin determination based on methylene blue detection by photothermal lens spectroscopy," *Anal. Biochem.*, vol. 594, no. January, p. 113621, 2020, doi: 10.1016/j.ab.2020.113621.

[29] M. Beyer, C. Hladun, and F. Bou-Abdallah, "Detection of proteins with ascorbic acid-capped gold nanoparticles: a simple and highly sensitive colorimetric assay," *Anal. Methods*, vol. 16, no. 31, 2024, doi: 10.1039/d4ay01146e.

[30] R. Wang, H. Wu, M. Qi, J. Han, and Z. Ren, "Bovine Serum Albumin Detection by Graphene Oxide Coated Long-Period Fiber Grating," *Photonic Sensors*, vol. 12, no. 3, pp. 1–10, 2022, doi: 10.1007/s13320-022-0649-6.